

# The current-voltage measurements under flat-top pulsed magnetic fields for non-ohmic transport study

Cite as: Rev. Sci. Instrum. 93, 085102 (2022); doi: 10.1063/5.0097702

Submitted: 30 April 2022 • Accepted: 10 July 2022 •

Published Online: 5 August 2022



View Online



Export Citation



CrossMark

Wenqi Wei,<sup>1,2</sup> Ming Yang,<sup>1</sup> Shimin Jin,<sup>1</sup> Haipeng Zhu,<sup>1</sup> Junfeng Wang,<sup>1</sup> and Xiaotao Han<sup>1,2,a)</sup>

## AFFILIATIONS

<sup>1</sup> Wuhan National High Magnetic Field Center, Huazhong University of Science and Technology, Wuhan 430074, China

<sup>2</sup> State Key Laboratory of Advanced Electromagnetic Engineering and Technology, Huazhong University of Science and Technology, Wuhan 430074, China

<sup>a)</sup>Author to whom correspondence should be addressed: [xthan@mail.hust.edu.cn](mailto:xthan@mail.hust.edu.cn)

## ABSTRACT

Investigation of the non-ohmic transport behaviors under high magnetic fields can provide a new way to explore novel field-induced phenomena. We present the current–voltage measurements under high magnetic fields based on the flat-top pulsed magnetic field system. Two different measurement strategies were compared, given that the excitation current swept continuously or increased by a series of pulses. For the short duration of the flat-top pulsed field, the continuous current method was adopted and well optimized to reduce the Joule heating and achieve the quasi-static measurements. Finally, the non-ohmic behaviors of a quasi-one-dimensional charge density wave  $\text{Li}_{0.9}\text{Mo}_6\text{O}_{17}$  were successfully studied under the magnetic field up to 30 T at 4.2 K, which was the first current–voltage measurements carried out in pulsed magnetic fields.

Published under an exclusive license by AIP Publishing. <https://doi.org/10.1063/5.0097702>

## I. INTRODUCTION

Magnetotransport studies, i.e., the transport properties such as the longitudinal and the Hall resistance in response to the magnetic field, represent one of the most powerful and straightforward tools to probe the electronic structure of conducting materials in condensed-matter physics.<sup>1</sup> Under a magnetic field, the orbital motion of charge carriers and the interactions involving the spins can generate a series of classical and quantum transport phenomena such as the magnetoresistance effect, the quantum Hall effect, quantum oscillations, and field-induced transitions.<sup>2–4</sup> Within recent decades, the developments of high field magnets have enabled the magnetotransport studies under extreme conditions and opened an avenue for exploring the band structure details in various electron systems such as superconductors, strongly correlated systems, low dimensional electron systems, and quantum topological matters.<sup>5–8</sup>

Nowadays, the ever-increasing demands on the performance of modern electronic devices and circuits require more investigations under nonequilibrium conditions. Along with the thoroughly investigated magnetoresistance under magnetic fields, another important

aspect of the transport properties is the electrical field response. According to Ohm's law, the voltage should be proportional to the current flowing through the sample, with the ratio being the resistance of the conductor. As a result, the current–voltage ( $I$ – $V$ ) characteristics should be linear, given that the resistance is independent of the electrical field. Under certain circumstances, the  $I$ – $V$  characteristics violate Ohm's law and become non-linear when the electrical field is high enough, given that the resistance is bias dependent. The non-ohmic transport behaviors have been widely observed and studied in metal oxides and organic charge-transfer salts.<sup>9–11</sup> The potential applications to switching and memory devices and the exploration on the more fundamental viewpoints of the conduction mechanism have been attracting tremendous increases in the community.

Among the commonly studied non-ohmic systems is the charge density wave (CDW), where the charge carriers develop a spatial modulation in the system.<sup>12</sup> The non-linear  $I$ – $V$  characteristics in quasi-one-dimensional CDW systems are attributed to the sliding mode of the CDW when the electrical field exceeds a threshold value  $E_T$ . A longstanding question is to study the many-body ground states and figure out the interactions under magnetic

fields. The non-ohmic transport studies under magnetic fields offer another approach to probe the CDW state and related properties. A typical example rises from the identification of the field-induced CDW phase in graphite under moderate magnetic field around 21 T.<sup>13</sup> Despite three decades of intense studies, it is still strongly desirable to perform the *I*-*V* measurements to get more insights of the pairing mechanism in the ultra-high magnetic field regime.<sup>14,15</sup>

The *I*-*V* measurements are now only realized in steady-state magnetic fields and limited by the field strength. To date, only the non-destructive pulsed magnets can generate strong pulsed magnetic fields higher than 45 T in milliseconds time scale<sup>16–19</sup> but are difficult to perform the *I*-*V* measurements. Since the rapid time-dependent field change in the pulsed magnetic field, the magnetocaloric effect and/or eddy current induced in the sample could disturb the *I*-*V* measurements. In addition, the unstable magnetic fields also could cause the phase transition in the sample during the process of measurements, and the results may be fuzzy. Most importantly, the short peak duration of the pulsed magnetic field is insufficient to carry out the *I*-*V* measurements by the conventional pulsed current technique.<sup>13,20–23</sup> To avoid the Joule heating disturbance, the *I*-*V* measurements require long enough cooling time intervals to sweep the current by using the pulse technique. Therefore, the *I*-*V* measurements are time-consuming and constrained within constant continuous magnetic fields.

In this work, we developed the *I*-*V* measurement system under pulsed magnetic fields in Wuhan National High Magnetic Field Center. Based on the flat-top pulsed magnetic field (FTPMF), an optimized continuous current method was applied in the *I*-*V* measurements. The non-linear *I*-*V* characteristic behaviors in a quasi-one-dimensional purple bronze  $\text{Li}_{0.9}\text{Mo}_6\text{O}_{17}$  were studied under FTPMF up to 30 T at 4.2 K.

## II. APPARATUS

### A. Flat-top pulsed magnetic field

To generate a stable magnetic field at the peak period of the pulsed field, the FTPMF technique has been developed in recent years.<sup>24–28</sup> Here, we used a compensation coil in the bore of pulsed magnet to regulate the magnetic field with a combined feedforward and feedback control.<sup>26</sup> The schematic illustration of the FTPMF system and the magnetic field profiles are shown in Figs. 1(a) and 1(b), respectively.

The main magnet, which has a bore diameter of 20 mm, an inductance of 3.5 mH, and a resistance of 44 mΩ at 77 K, was powered by the capacitor banks  $C_m$  (the single capacitor bank is 3.84 mF and can be charged up to 1.2 MJ) to produce the pulsed high magnetic field. The magnetic field of this kind of magnet can reach 65 T depending on the discharging energies of the driven capacitor banks.

A compensation coil made of 0.4 mm copper wires was double wound around a 17 mm Helium cryostat tail and reinforced by a Zylon/epoxy composite layer of 0.5 mm thickness. The compensation coil was immersed in liquid nitrogen at 77 K and powered by twelve 12-V lead-acid batteries in series to generate an adjustable magnetic field from 0 to 1 T beyond 5 ms. The current of the compensation coil was regulated by an insulated gate bipolar transistor

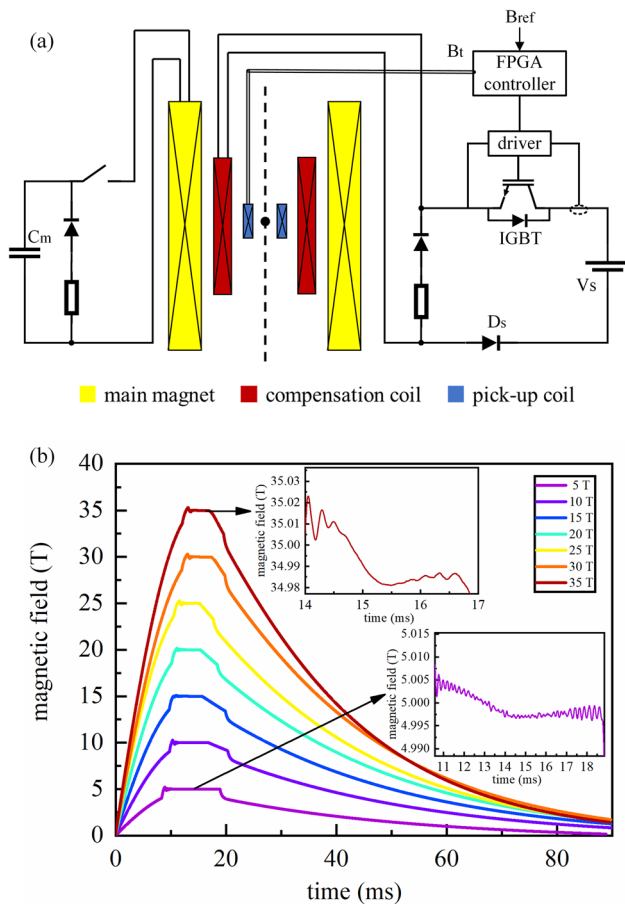


FIG. 1. (a) Schematic illustration of the FTPMF system. (b) Magnetic field profiles generated by the constructed flat-top system.

(IGBT, FZ3600R17KE3-B2, Infineon) with a homemade driver that can linearize the transfer characteristic of the IGBT through the current feedback. A field-programmable gate array (FPGA) controller cRIO-9063 with an analog input module NI-9215 and a bidirectional digital module NI-9401 (National Instruments) was employed to acquire the magnetic field signal  $B_t$  from the pick-up coil, carry out proportional-integral-derivative (PID) control as well as feed-forward correction with the reference signal  $B_{ref}$ , and output control signals to the IGBT driver every 10 μs. A diode  $D_s$  was applied to avoid the opposite current heating of the compensation coil caused by the large electromagnetic induction at the rising period of the main magnetic field.

To increase the peak time and decrease the sweep rate of the main pulsed field, 6/8 parallel capacitor banks were applied. Highly stable flat-top pulsed magnetic fields up to 35 T were produced, whose stability was within ±5 to ±20 mT, and the duration was within 3–8 ms depending on the field strength. Due to the regulating capability limitation of the compensation coil, higher flat-top fields were not successfully achieved.

**B. *I*-*V* measurement circuit**

Due to the short flat-top duration of the pulsed magnetic field, a high-speed *I*-*V* measurement circuit was developed, which is shown in Fig. 2. For rapid current excitation and data collection, a PXIe-1062Q chassis containing PXI-5412 waveform generator and PXI-5105 oscilloscope (National Instruments) was employed. The PXI-5412 waveform generator could function as an arbitrary voltage source with a wide voltage range from  $\pm 2.82$  mV to  $\pm 6$  V in  $50\ \Omega$  loads. A ballast resistor  $R_b$  with the large resistance connected with the sample in series was applied for the voltage-to-current converter and stabilized the excitation current regardless of the resistance change of the sample. The current in the circuit was detected by measuring the voltage drop  $U_I$  through a small and precise sampling resistor  $R_i$ , which was also connected in series with the sample. The sample voltage signal  $U_V$  and current signal  $U_I$  were filtered and amplified by the SR560 low-noise preamplifiers (Stanford Research) and finally were acquired by the 12-bit oscilloscope PXI-5105 with the sample rate of 5 MS/s. To achieve the *I*-*V* measurements at different temperatures, a Model 335 temperature controller (LakeShore Cryotronics) was implemented with a thermometer and heater mounted on the probe around the sample.

**C. Probe of sample**

Figure 3(a) shows the sketch of the homemade low temperature probe, which was located at the center of the main magnet and

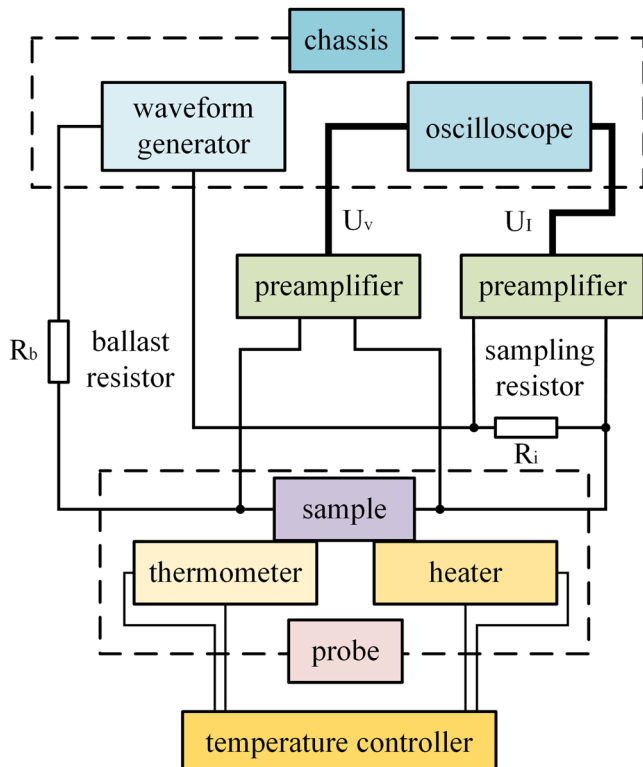


FIG. 2. Block diagram of the high-speed *I*-*V* measurement circuit.

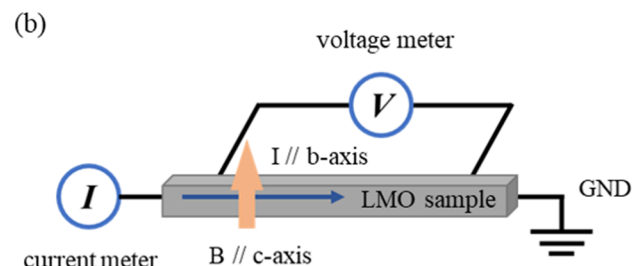
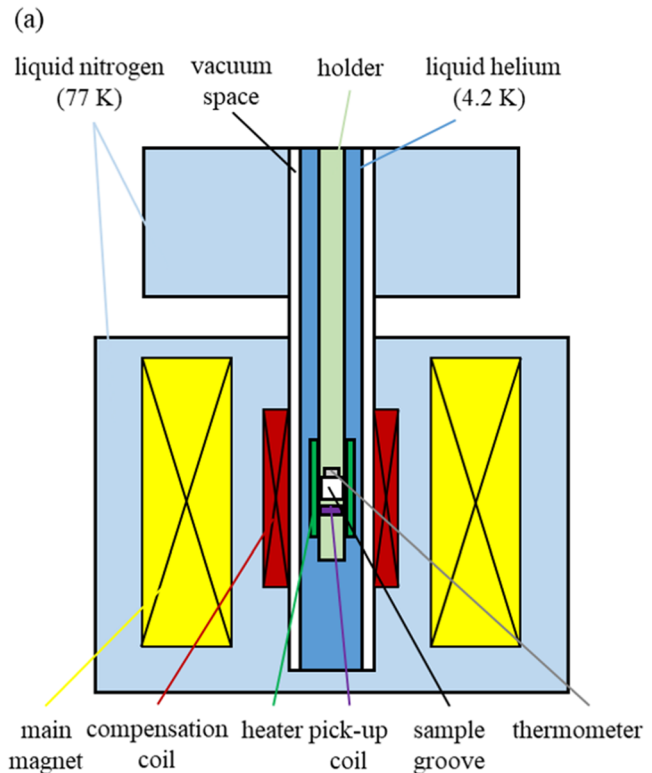


FIG. 3. (a) Sketch of the homemade low temperature probe system. (b) The *I*-*V* measurement connection of the sample by using the four-probe technique.

the compensation coil. The sample holder was made of the non-metallic compound material G10 and engraved at its bottom for placing the sample, which was immersed in 4.2 K liquid helium and surrounded by the heater. The thermometer and the pick-up coil were located close to the sample as possible to acquire precise temperature and magnetic field signals. The He cryostat had vacuum space to maintain an adiabatic condition and used 77 K liquid nitrogen as a jacket layer to reduce the evaporation rate of the liquid helium.

High quality single crystal of  $\text{Li}_{0.9}\text{Mo}_6\text{O}_{17}$  (LMO) was to be studied under high fields, since the obvious non-ohmic transport characteristics at low temperature had been previously observed.<sup>29</sup> Figure 3(b) shows the scheme of the sample connection for the *I*-*V* measurements by using the four-probe technique. To bypass the influence of contact resistance, the voltage meter was connected to

the surface of the sample instead of the current wires. The excitation current  $I$  was applied parallel to the  $b$ -axis of the sample, and the magnetic field was parallel to the  $c$ -axis.

### III. METHOD

#### A. Continuous current method

To accomplish the  $I$ - $V$  measurements during the short flat-top of the high field, a single triangle-wave current pulse was applied, as shown in Fig. 4. The first rising part of the continuous current after the trigger was used for the  $I$ - $V$  measurements. Since the Joule heating occurs when the current flows through the sample, the pulse rising time  $t_r$  should be as short as possible. However, high-frequency parasitic parameters can disturb the intrinsic transport measurement, and the real current cannot follow the track of command when the pulse rises too quickly. To reduce the effect of the Joule heating and realize quasi-static measurements as possible, the appropriate  $t_r$  was need to be determined.

#### B. Pulsed current method

To eliminate the heating effect disturbance, the pulsed current method has been widely used in the  $I$ - $V$  measurements for decades,<sup>13,20–23</sup> which is shown in Fig. 5. The applied current is a series of rectangular pulses with the increasing amplitude  $\Delta I$ . The single pulse duration  $t_s$  and the interval cooling time  $t_c$  need to be long enough to make sure the circuit reaches its equilibrium and the sample recovers initial temperature. To further reduce heating errors in every single pulse, the sampling points should be selected at the beginning of each real current pulse reaching the state after the electrical transient instead of the thermal transient. Compared with the continuous current method, the pulsed current method is more accurate but time-consuming. It is more suitable for steady continuous magnetic fields or long flat-top pulsed magnetic fields.

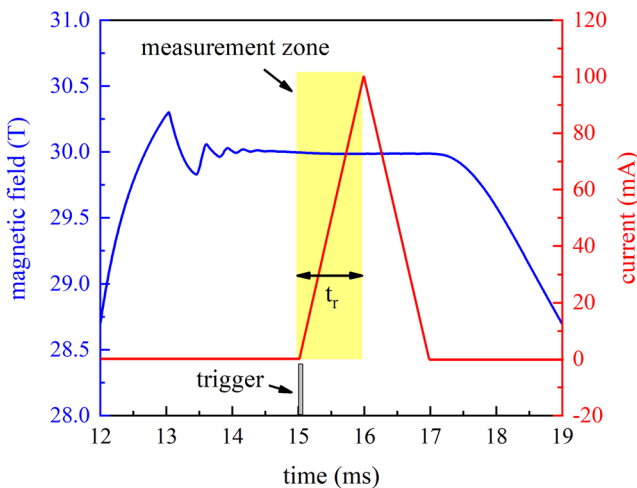


**FIG. 4.** Profile of the continuous current method applied for the  $I$ - $V$  measurements during the short flat-top of high field.

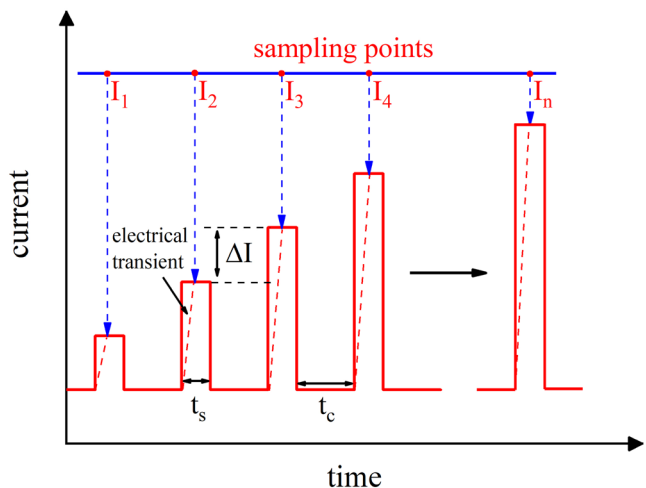


**FIG. 5.** The pulsed current method for reducing the heating effect. The sampling points were selected at the beginning of each real current pulse reaching the state after the electrical transient instead of the thermal transient.

#### C. Optimization of the measurement strategy

Under the conditions of 4.2 K and 0 T, the  $I$ - $V$  measurements of the LMO were achieved by the continuous current method at different current rising time  $t_r$ . The results were plotted and compared in Fig. 6. During the continuous current measurements,  $t_r$  varied from 0.1 to 5 ms, and the current amplitude increased continuously up to 100 mA. For all the values of  $t_r$ , the voltage vs current curves present ohmic behavior up to a threshold current, beyond which is followed by the negative differential resistance (NDR) phenomenon ( $dV/dI < 0$ ). However, the onset of the NDR shifts to lower current as  $t_r$  increases, as well as the resistance of the sample decreases, which is extracted from the value of  $I$ - $V$ . It is thus reasonable to conclude that for longer  $t_r$ , the heating effect is much more pronounced than the shorter ones since the resistance decreases as the temperature increases in the vicinity of 4.2 K.<sup>29</sup>

The pulsed current method was used for comparison. To determine the proper measurement strategy, the current and voltage responses of the sample excited by a single rectangular pulse were measured. Clearly, a nonequilibrium process occurred as shown in Fig. 7, which could be divided into an electrical transient (yellow part) and a thermal transient (green part). The first transient was caused by the parasitic parameters of the measurement circuit such as the inductance and the capacitance, which lasted nearly 20  $\mu$ s. The second transient beyond 200  $\mu$ s was caused by the Joule heating, which led to the decrease of the resistance of the sample. For the pulsed current method, the appropriate sampling zone should be the transition between the two transients (gray part). It is noteworthy that the labeled gray zone only ensures that the measurement errors from the electrical transient and the thermal effect were reduced but not well minimized. Nevertheless, the present sampling strategy could ensure that the measurements were not heavily affected by the two effects to some extent. A series of rectangular current pulses with  $\Delta I$  of 1 mA were finally applied, whose  $t_s$  and  $t_c$  were set to 0.5 and 3 ms, respectively, according to the maximum current pulse test of

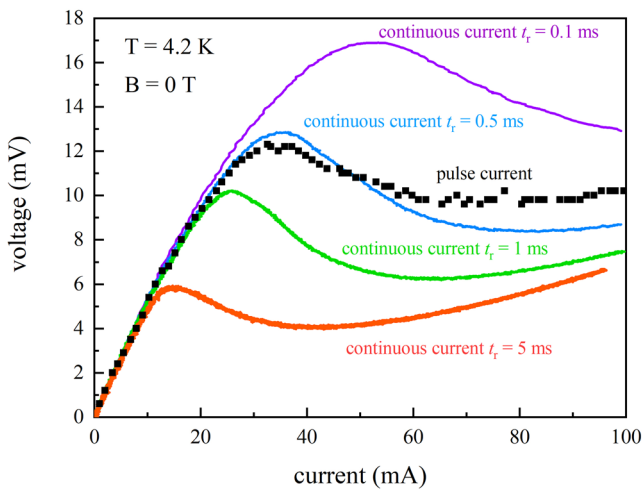


**FIG. 6.** The  $I$ - $V$  measurements of the LMO performed by the continuous current method (solid lines) at different current rising time  $t_r$ , and the pulsed current method (dotted line) under the conditions of 4.2 K and 0 T. The continuous current of  $t_r = 0.5$  ms was finally adopted in the  $I$ - $V$  measurements under the pulsed field.

100 mA. The voltage vs current curve was also plotted as black scatterers in Fig. 6. It is revealed that the sample behavior captured by the pulsed current method is in good agreement with that measured by the continuous current method with  $t_r = 0.5$  ms. It is noted that the onset of NDR shifts to higher current and the resistance increases for the shorter one of  $t_r = 0.1$  ms, which can be explained as the measurement in the electrical transient caused by parasitic electrical parameters.

#### IV. RESULTS

Before the pulsed field measurements, the basic  $I$ - $V$  characteristics of LMO sample 1<sup>#</sup> were first checked in a Physical Property

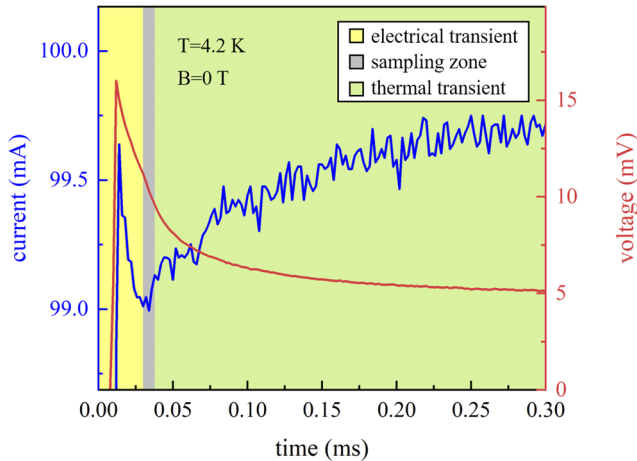


**FIG. 7.** Current (blue line) and voltage (red line) responses of the sample excited by a single rectangular pulse. The nonequilibrium process was divided into the electrical transient (yellow part) and the thermal transient (green part). The transition between the two transients was the appropriate sampling zone (gray part).

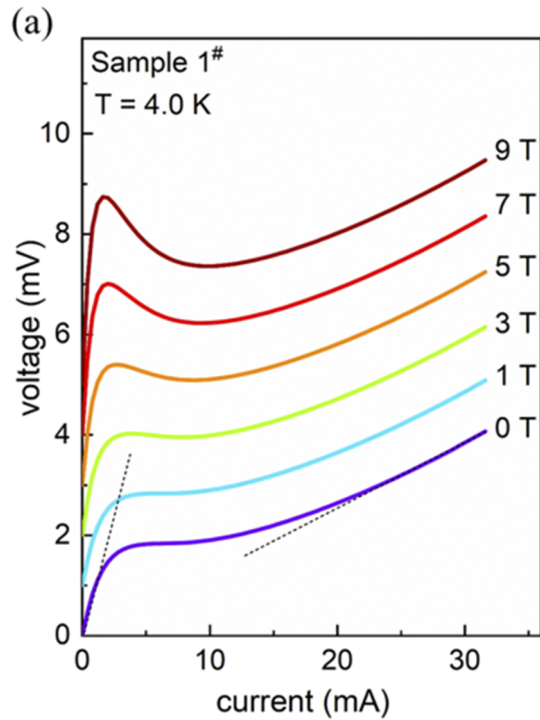


**FIG. 8.** (a) The  $I$ - $V$  curves of the sample measured by PPMS at 4.0 K. (b) The  $I$ - $V$  curves of the sample measured with the flat-top field up to 30 T at 4.2 K. The 50 T data were obtained under a pulsed field without the flat-top. Data are shifted for clarity. The dashed lines are a guideline for the linear  $I$ - $V$  transport properties.

Measurement System (PPMS) under steady-state fields up to 9 T at 4.0 K. The data were plotted in Fig. 8(a) and shifted for clarity. At zero field  $B = 0$  T, the  $I$ - $V$  curve is obviously non-linear. For the very low current range, the voltage increases linearly with the current until the current reaches around 2 mA. The slope of the  $I$ - $V$  curve dramatically decreases and the curve deviates from the linear (dashed line). As the current increases further, the  $I$ - $V$  behavior returns to be linear with a much smaller slope compared to the low current regime. When the field is increased, the non-linearity becomes more pronounced and the negative differential resistance behavior appears in the moderate current range. The non-linear  $I$ - $V$  behavior is reminiscent of the S-like  $I$ - $V$  characteristics observed in other one-dimensional CDW systems<sup>30,31</sup> and can be attributed to the sliding state of the CDW in LMO.

The high field  $I$ - $V$  characteristics were performed in FTPMF by using the continuous current method with  $t_r = 0.5$  ms. Figure 8(b) shows the  $I$ - $V$  curves of another LMO sample (denoted as 2<sup>#</sup>) under the flat-top field up to 30 T at 4.2 K. In addition, we have also conducted the measurement under a normal pulsed field of 50 T for a comparison. It is worth noting that although the flat-top is not available for 50 T currently, the fast current sweeping time makes sure that the magnetic field is approximately constant. The magnetic field fluctuation is within 0.07 T during a time scale of 0.5 ms for the 50 T pulse. Furthermore, from our previous studies, the magnetoresistance at 50 T within a 0.07 T range is less than  $10^{-4}$ . Thus, we conclude that the  $I$ - $V$  curve measured under 50 T is also reliable and valid.

The NDR behavior is discernible for the measured magnetic field. The NDR behavior at zero field is more pronounced in sample 2<sup>#</sup> due to the sample dependence. It is interesting that the onset of the NDR develops as the magnetic field is increased. In addition, the NDR effect is also obviously enhanced as the field increases up to 15 T. As the field is further increased, the NDR is strongly suppressed and becomes weak at  $B = 50$  T. The field dependence of the NDR behavior is in good agreement with the data in magnetoresistivity that a peak appears around 15 T.<sup>29</sup> At  $B = 0$  T, the linear  $I$ - $V$  behavior in the low current regime is a manifestation of the transport contribution of the remaining normal carriers in the CDW state. As the current increases, the CDW gap overcomes and the frozen carriers start to contribute to the transport, and thus the NDR appears. The enhancement of the NDR under low magnetic field ( $B < 15$  T) can be explained by the magnetic field-induced CDW transition as observed in similar systems. In the high field regime, the NDR effect is strongly suppressed probably due to the CDW damping by the magnetic field. Although a detailed theoretical understanding of the NDR is still lacking, the NDR behavior and its evolution with magnetic field are perhaps related to the magnetic field modulation on the CDW state in LMO, given that the carrier density increases significantly due to the collective depinning of the density wave. More theoretical and experimental investigations under higher fields are desirable to reveal the underlying mechanisms.

## V. DISCUSSION

Due to the narrow bore diameter of the main magnet, the compensation coil had a small wire diameter, which led to a large resistance. It means that more batteries were needed to produce

the same regulated magnetic field, and the Joule heating of the coil was heavier to cause the degradation of regulating capability compared to one of larger wire diameter. With the limitation of power voltage, the field decoupling coil<sup>26</sup> was not wound in our present design. When the main magnetic field changed more quickly with the gradual increase of field strength, higher mutual inductance voltage interference was induced in the circuit of the compensation coil, which caused the instability of the flat-top control system. Therefore, higher flat-top pulse fields beyond 40 T were not successfully produced in the present experiment. A magnet with the larger bore diameter or more batteries in series for the decoupled compensation coil will improve the strength of the flat-top magnetic field.

Presently, the maximum measurement current is less than 100 mA. However, for a wider range of  $I$ - $V$  measurements, a power amplifier can be added in the post stage of the waveform generator, which means the thermal stability of the  $I$ - $V$  measurement circuit needs further consideration.

It is noted that the continuous current method still suffers from the heating effect when the current is large, as shown in Fig. 6. If the parasitic electrical parameters of measuring ports can be obtained exactly, the electrical transient error can be well corrected, and more quickly continuous current can be carried out to further reduce the influence of the Joule effect.

## VI. CONCLUSION

In this paper, we report the development of the current–voltage measurements system in pulsed magnetic fields. Based on the flat-top pulsed magnetic field up to 30 T, the non-ohmic transport behaviors of  $\text{Li}_{0.9}\text{Mo}_6\text{O}_{17}$  were performed with the high-speed measurement circuit and low temperature probe by using the continuous current method. To reduce the Joule heating and achieve quasi-static measurements, the rising time of the continuous current was corrected with comparison of the pulsed current method. Although the flat-top field strength is limited at present, our results open up the possibilities for the accurate  $I$ - $V$  characteristics investigation under very high magnetic fields.

## ACKNOWLEDGMENTS

This work was supported by the National Natural Science Foundation of China (Grant Nos. 12004122 and 51821005).

## AUTHOR DECLARATIONS

### Conflict of Interest

The authors have no conflicts to disclose.

### Author Contributions

**Wenqi Wei:** Methodology (lead); Visualization (lead); Writing – original draft (equal). **Ming Yang:** Resources (lead); Writing – original draft (equal). **Shimin Jin:** Investigation (lead). **Haipeng Zhu:** Data curation (lead). **Junfeng Wang:** Conceptualization (lead); Supervision (equal). **Xiaotao Han:** Conceptualization (equal); Project administration (lead).

## DATA AVAILABILITY

The data that support the findings of this study are available from the corresponding author upon reasonable request.

## REFERENCES

- <sup>1</sup>D. Shoenberg, *Magnetic Oscillations in Metals* (Cambridge University Press, Cambridge, 1984).
- <sup>2</sup>L. Schubnikow and W. J. De Haas, *Nature* **126**, 500 (1930).
- <sup>3</sup>K. V. Klitzing, G. Dorda, and M. Pepper, *Phys. Rev. Lett.* **45**, 494 (1980).
- <sup>4</sup>F. Lévy, I. Sheikin, B. Grenier, and A. D. Huxley, *Science* **309**, 1343 (2005).
- <sup>5</sup>N. Doiron-Leyraud, C. Proust, D. LeBoeuf, J. Levvallois, J.-B. Bonnemaison, R. Liang, D. A. Bonn, W. N. Hardy, and L. Taillefer, *Nature* **447**, 565 (2007).
- <sup>6</sup>H. Wang, H. Liu, Y. Li, Y. Liu, J. Wang, J. Liu, J.-Y. Dai, Y. Wang, L. Li, J. Yan, D. Mandrus, X. C. Xie, and J. Wang, *Sci. Adv.* **4**, eaau5096 (2018).
- <sup>7</sup>Z. Xiang, Y. Kasahara, T. Asaba, B. Lawson, C. Tinsman, L. Chen, K. Sugimoto, S. Kawaguchi, Y. Sato, G. Li, S. Yao, Y. L. Chen, F. Iga, J. Singleton, Y. Matsuda, and L. Li, *Science* **362**, 65 (2018).
- <sup>8</sup>S. Ran, I.-L. Liu, Y. S. Eo, D. J. Campbell, P. M. Neves, W. T. Fuhrman, S. R. Saha, C. Eckberg, H. Kim, D. Graf, F. Balakirev, J. Singleton, J. Paglione, and N. P. Butch, *Nat. Phys.* **15**, 1250 (2019).
- <sup>9</sup>J. Z. Sun, L. Krusin-Elbaum, P. R. Duncombe, A. Gupta, and R. B. Laibowitz, *Appl. Phys. Lett.* **70**, 1769 (1997).
- <sup>10</sup>A. Asamitsu, Y. Tomioka, H. Kuwahara, and Y. Tokura, *Nature* **388**, 50 (1997).
- <sup>11</sup>Y. Iwasa, T. Koda, S. Koshihara, Y. Tokura, N. Iwasawa, and G. Saito, *Phys. Rev. B* **39**, 10441(R) (1989).
- <sup>12</sup>G. Grüner, *Rev. Mod. Phys.* **60**, 1129 (1988).
- <sup>13</sup>Y. Iye and G. Dresselhaus, *Phys. Rev. Lett.* **54**, 1182 (1985).
- <sup>14</sup>F. Arnold, A. Isidori, E. Kampert, B. Yager, M. Eschrig, and J. Saunders, *Phys. Rev. Lett.* **119**, 136601 (2017).
- <sup>15</sup>Z. Zhu, P. Nie, B. Fauqué, B. Vignolle, C. Proust, R. D. McDonald, N. Harrison, and K. Behnia, *Phys. Rev. X* **9**, 011058 (2019).
- <sup>16</sup>R. Battesti, J. Beard, S. Böser, N. Bruyant, D. Budker, S. A. Crooker, E. J. Daw, V. V. Flambaum, T. Inada, I. G. Irastorza, F. Karbstein, D. L. Kim, M. G. Kozlov, Z. Melhem, A. Phipps, P. Pugnat, G. Rikken, C. Rizzo, M. Schott, Y. K. Semertzidis, H. H. J. ten Kate, and G. Zavattini, *Phys. Rep.* **765-766**, 1 (2018).
- <sup>17</sup>J. Singleton, C. H. Mielke, A. Migliori, G. S. Boebinger, and A. H. Lacerda, *Physica B* **346-347**, 614 (2004).
- <sup>18</sup>T. Peng, F. Jiang, Q. Q. Sun, Q. Xu, H. X. Xiao, F. Herlach, and L. Li, *IEEE Trans. Appl. Supercond.* **24**, 4300604 (2014).
- <sup>19</sup>J. Beard, J. Billette, N. Ferreira, P. Frings, J.-M. Lagarrigue, F. Lecouturier, and J.-P. Nicolin, *IEEE Trans. Appl. Supercond.* **28**, 4300305 (2018).
- <sup>20</sup>C. Canali, G. Majni, R. Minder, and G. Ottaviani, *IEEE Trans. Electron Devices* **22**, 1045 (1975).
- <sup>21</sup>B. Fisher, J. Genossar, K. B. Chashka, L. Patlagan, and G. M. Reisner, *Appl. Phys. Lett.* **88**, 152103 (2006).
- <sup>22</sup>T. Mori, Y. Bando, T. Kawamoto, I. Terasaki, K. Takimiya, and T. Otsubo, *Phys. Rev. Lett.* **100**, 037001 (2008).
- <sup>23</sup>H. Li, J. Wang, R. Xiong, F. Yi, W. Tang, Z. Yu, and J. Shi, *Mod. Phys. Lett. B* **18**, 697 (2004).
- <sup>24</sup>L. J. Campbell, H. J. Boenig, D. G. Rickel, J. B. Schillig, H. J. Schneider-Muntau, and J. R. Sims, *Physica B* **216**, 218 (1996).
- <sup>25</sup>F. Jiang, T. Peng, H. Xiao, J. Zhao, Y. Pan, F. Herlach, and L. Li, *Rev. Sci. Instrum.* **85**, 045106 (2014).
- <sup>26</sup>Y. Kohama and K. Kindo, *Rev. Sci. Instrum.* **86**, 104701 (2015).
- <sup>27</sup>S. Zhang, Z. Wang, T. Ding, H. Xiao, J. Xie, and X. Han, *IEEE Trans. Power Electron.* **35**, 2436 (2020).
- <sup>28</sup>S. Wang, T. Peng, F. Jiang, S. Jiang, S. Chen, L. Deng, R. Huang, and L. Li, *IEEE Trans. Appl. Supercond.* **30**, 4900404 (2020).
- <sup>29</sup>J. Z. Ke, C. Dong, H. P. Zhu, W. X. Liu, M. Y. Shi, Y. Q. Du, J. F. Wang, and M. Yang, *Ceram. Int.* **47**, 25229 (2021).
- <sup>30</sup>R. Xiong, D. Li, J. Wang, C. Li, W. Tang, and J. Shi, *Solid State Commun.* **142**, 251 (2007).
- <sup>31</sup>S. Martin, R. M. Fleming, and L. F. Schneemeyer, *Phys. Rev. B* **38**, 5733 (1988).